Supplementary Material

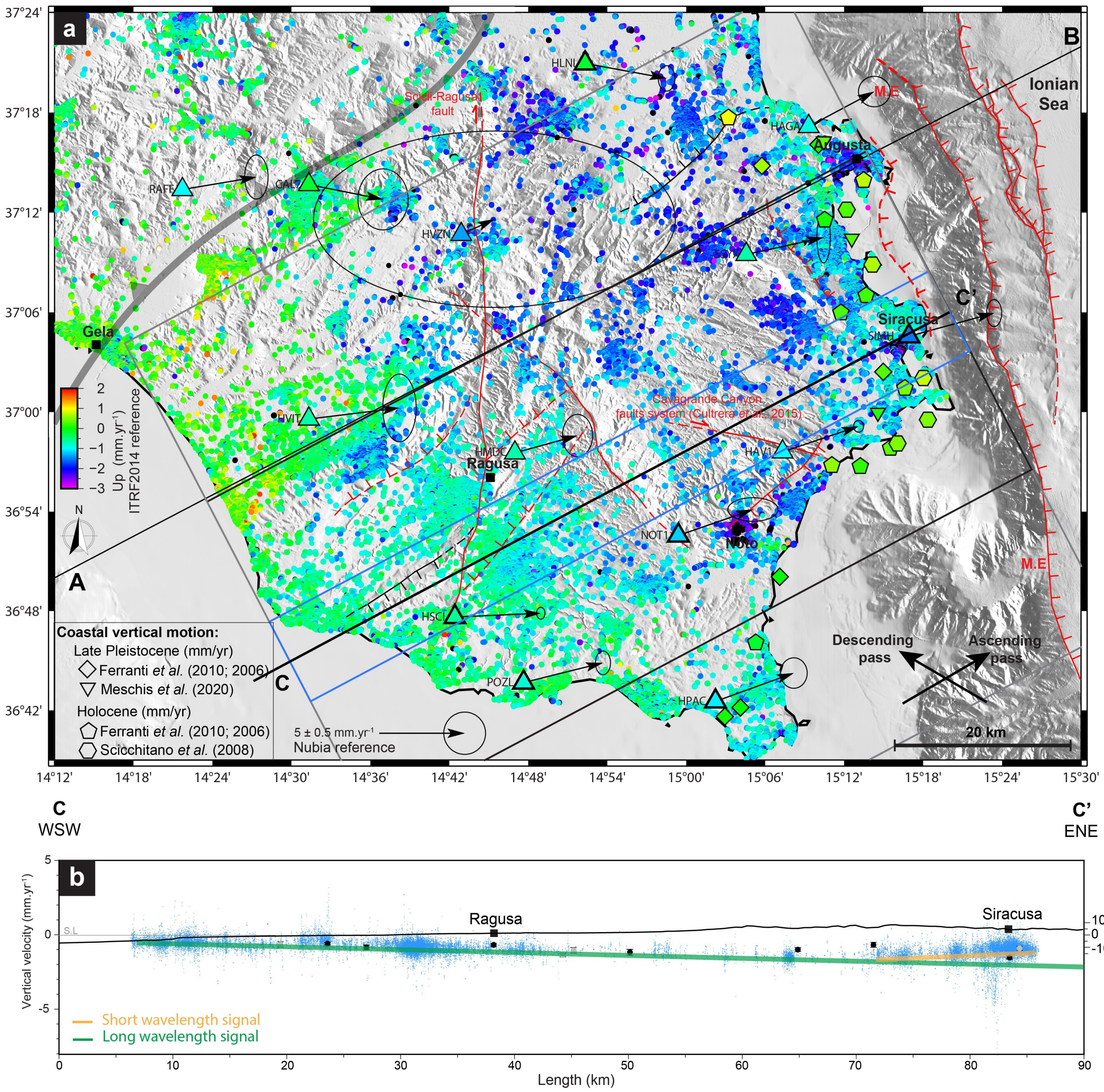

***Supplementary Figure S1**: Geodetics data available across the Hyblean Plateau region (see location in Figure 3). The Permanent-Scatterer (PS-InSAR) pseudo-3D Up velocities are from Henriquet et al., 2022 and are measured using Sentinel-1 satellite ascending and descending orbits acquired during the 2015-2020 period. GNSS 3D surface velocities were derived from a reanalysis of the Nevada Geodetic Laboratory (NGL) data including the time series of year 2023 (Horizontal components reference: fixed Nubia; Up components reference: ITRF2014). Coastal vertical motion during the Late Pleistocene and Holocene from Ferranti et al. (2006, 2010), Meschis et al. (2020), and Scicchitano et al. (2008). Major faults of the Hyblean Plateau and Malta Escarpment (M.E) including the offshore normal faults identified by Gutscher et al. (2016) and analyzed by Gambino et al. (2021) (red: active fault; red dashed: inferred active fault; black: inactive fault). SW-NE trending velocity profile showing surface velocity (Up) derived from PS-InSAR and GNSS stations vertical velocities (Up). PS-InSAR data were stacked across a 5 km width on both sides of the CC' profile (in blue). GNSS data were stacked using a 20 km (in black) and 40 km (in gray) widths on both sides of the CC' profile. Like for AB profile (Figure 2b), vertical velocities shown a long-wavelength signal (green line) and a short-wavelength signal in the East of Hyblean Plateau (orange line). Topographic and bathymetric profiles are presented without vertical exaggeration (V.E.x1).*

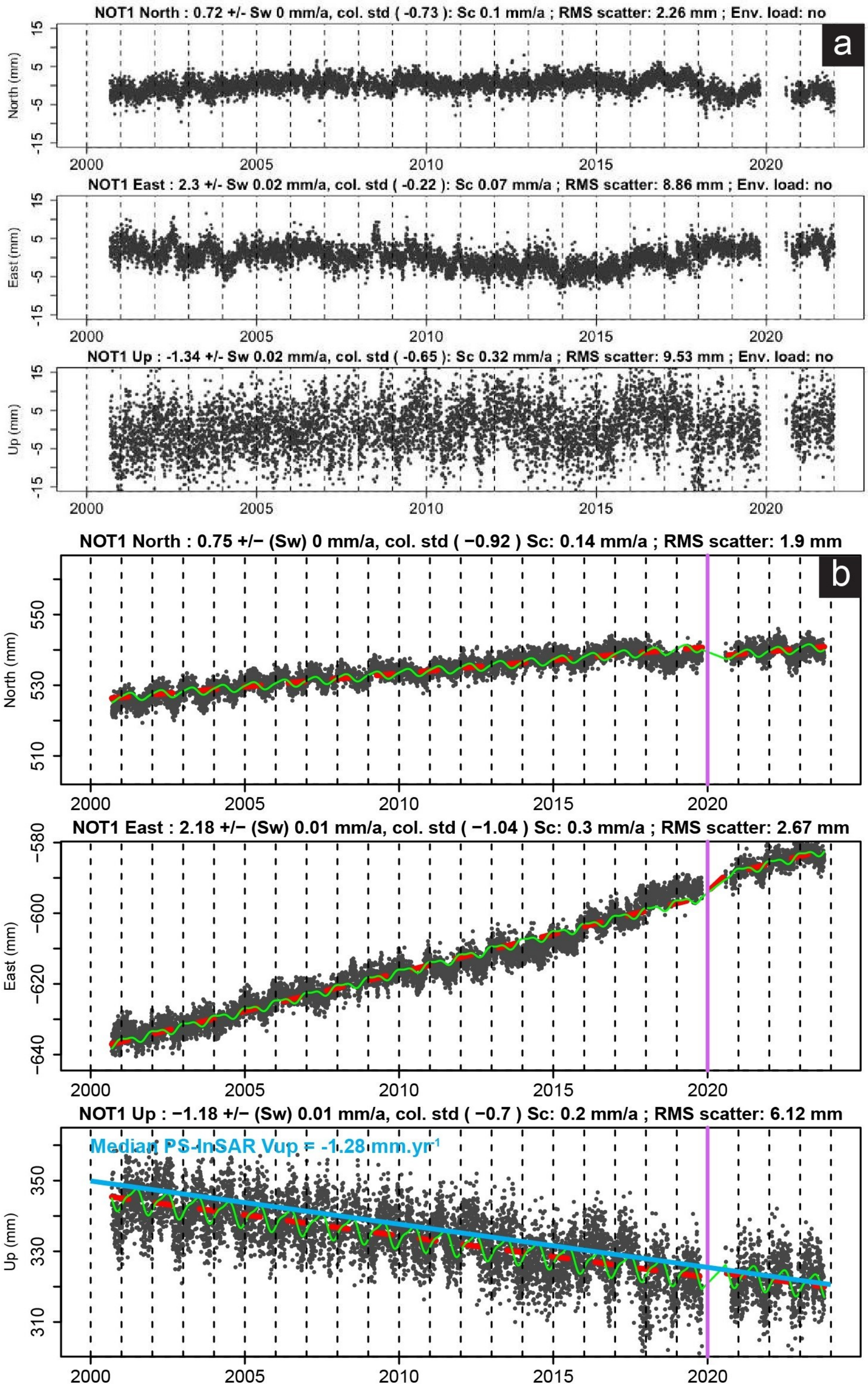

Supplementary Figure S2: *a) Raw time series of the NOT1 GNSS station for the North, East and Up components. b) Time series models of the NOT1 GNSS station for the North, East and Up components using inversion software from Masson et al., 2019. Linear trend appears in red. Periodic or seasonal and pluriannual effects are in green. Corrected offsets are indicated by a purple vertical line. Data configuration above the signals: GPS station name; component (North, East or Up); velocity (mm/yr); white noise (Sw); noise color; colored noise (Sc); dispersion (RMS). GNSS time series were obtained from the Nevada Geodetic Laboratory (Blewitt et al., 2018). PS-InSAR vertical velocities (see Figure 2) are extracted over 8 km^2 from the NOT1 station so that its median is correlated with the time series of the vertical component of NOT1 station.*

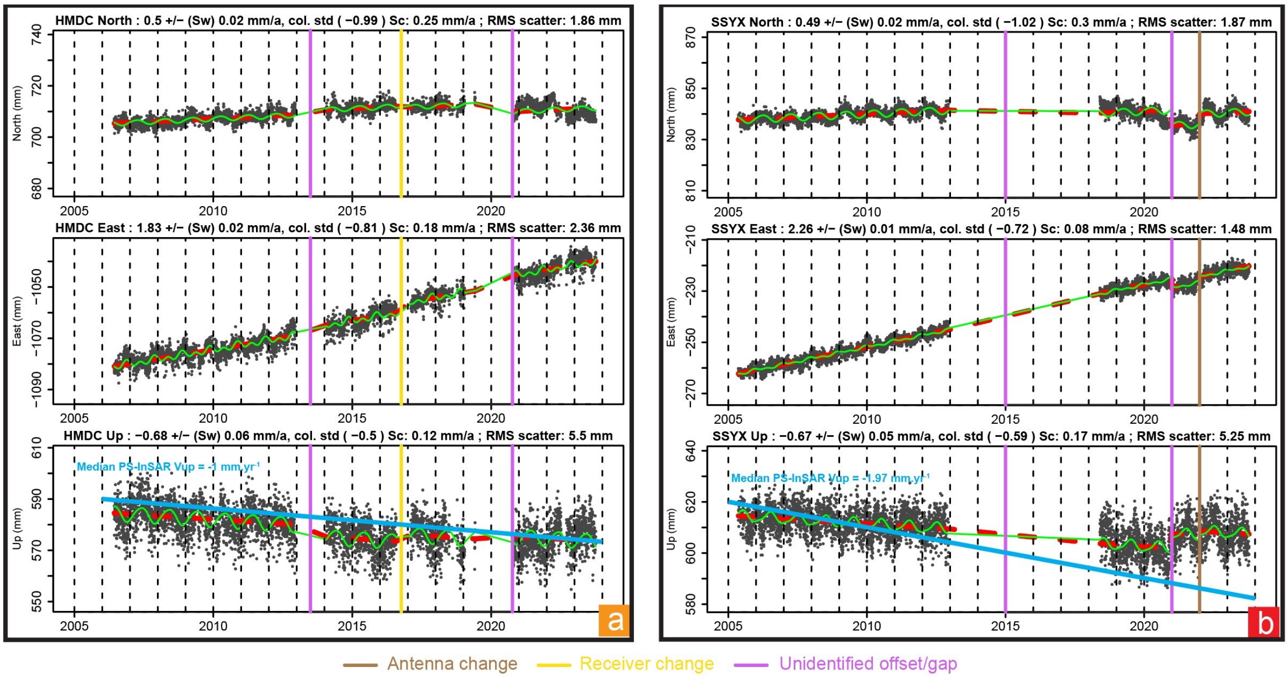

Supplementary Figure S3: *Time series models of a) the HMDC GNSS station (shown in orange square for the medium-quality of the time serie); b) the SSYX GNSS station (shown in red square for the doubtful-quality of the time serie) for the North, East and Up components using inversion software from Masson et al., 2019. Linear trend in red. Periodic or seasonal and pluriannual effects in green. Offset and/or gap are identified by receiver or antenna changes from Fabian et al., 2021. Data configuration above the signals: GPS station name; component (North, East or Up); velocity (mm/yr); white noise (Sw); noise color; colored noise (Sc); dispersion (RMS). Displacement data from the Nevada Geodetic Laboratory (Blewitt et al., 2018). PS-InSAR vertical velocities (see Figure 2) are extracted over 8 km^2 from the SSYX and HMDC stations so that its median is correlated with the time series of the vertical component of these GNSS stations.*

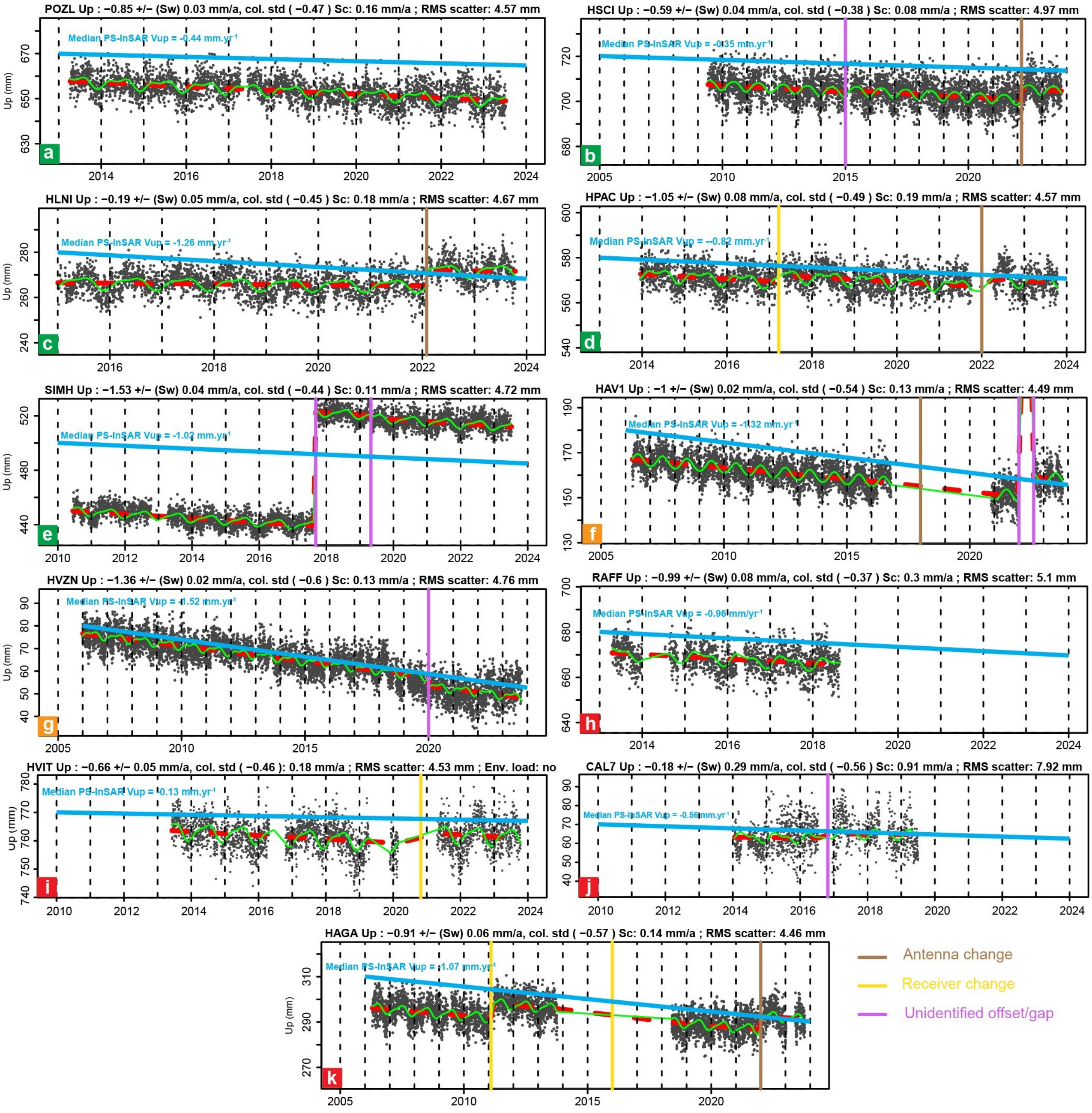

Supplementary Figure S4: *a-e) Good-quality time series (> 8 years, few gaps and offsets) (represented by a green square here and a thick GNSS station boundary in Figure 2a); f-g) Medium-quality time series (> 8 years with some gaps of several years and few offsets) shown in orange square; h-k) Doubtful-quality time series (gaps of several years and high scattering) shown in red square; models of GNSS station Up components using inversion software from Masson et al., 2019. Linear trend in red. Periodic or seasonal and pluri-annual effects in green. Corrected offsets are indicated by a purple vertical line. Offset and/or gap are identified by receiver or antenna changes from Fabian et al., 2021. Data configuration above the signals: GNSS station name; component (North, East or Up); velocity (mm/yr); white noise (Sw); noise color; colored noise (Sc); dispersion (RMS). Displacement data from the Nevada Geodetic Laboratory (Blewitt et al., 2018). PS-InSAR vertical velocities (see Figure 2) are extracted over 8 km^2 from the GNSS stations so that its median is correlated with the time series of the vertical component of these GNSS stations.*

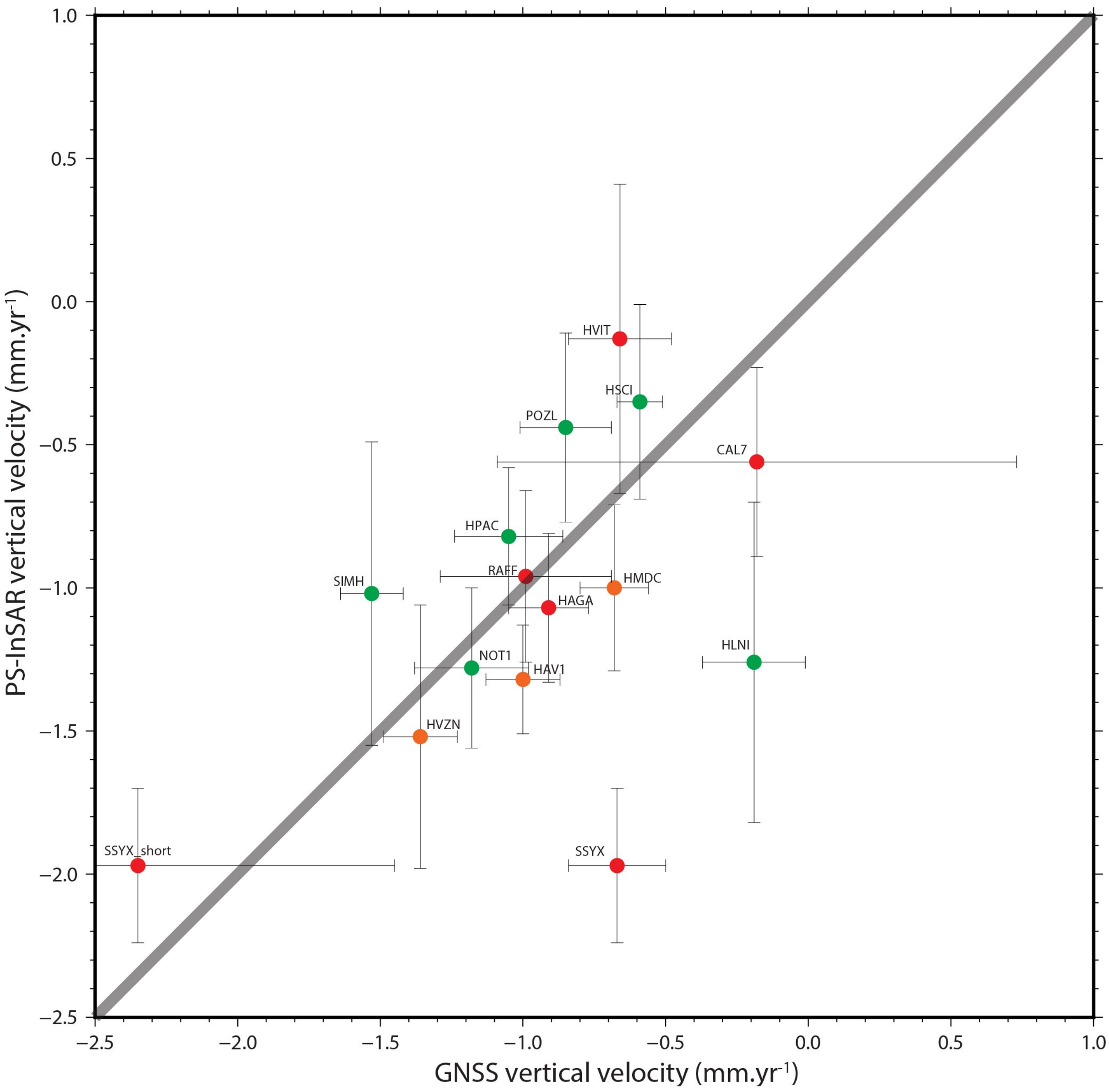

Supplementary Figure S5: *Correlation between GNSS vertical velocity models and median of PS-InSAR vertical velocities (see Figure 2) extracted over 8 km² from the GNSS stations. The uncertainty of PS-InSAR data is calculated with the average standard deviation of PS-InSAR data over 8 km² around the GNSS station. In green is the good-quality time series (> 8 years, few gaps and offsets), in orange is the medium-quality time series (> 8 years, few gaps of several years and few offsets), and in red is the doubtful-quality time series (gaps of several years and high scattering). The SSYX_short means the SSYX time series of 2018-2023.*

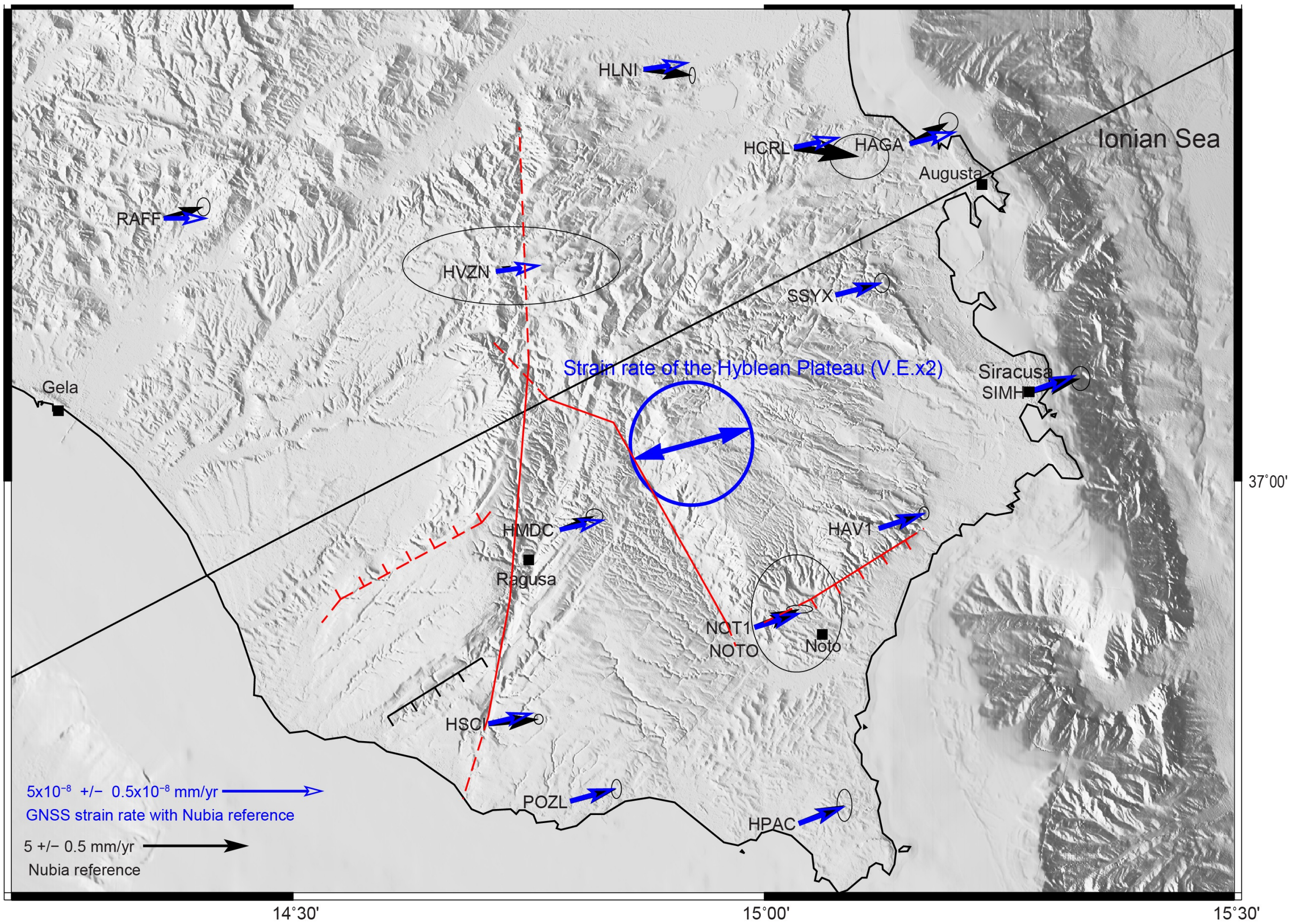

Supplementary Figure S6: *Strain rate inversion of GNSS horizontal components (Figure 3) using the Mazzotti et al. (2005) software. Comparison between the GNSS strain rate inversion (blue vectors) and the GNSS horizontal component models (black vectors) for each GNSS station of Hyblean Plateau. Global GNSS strain rate inversion of the Hyblean Plateau has a horizontal exaggeration (V.E.x2).*

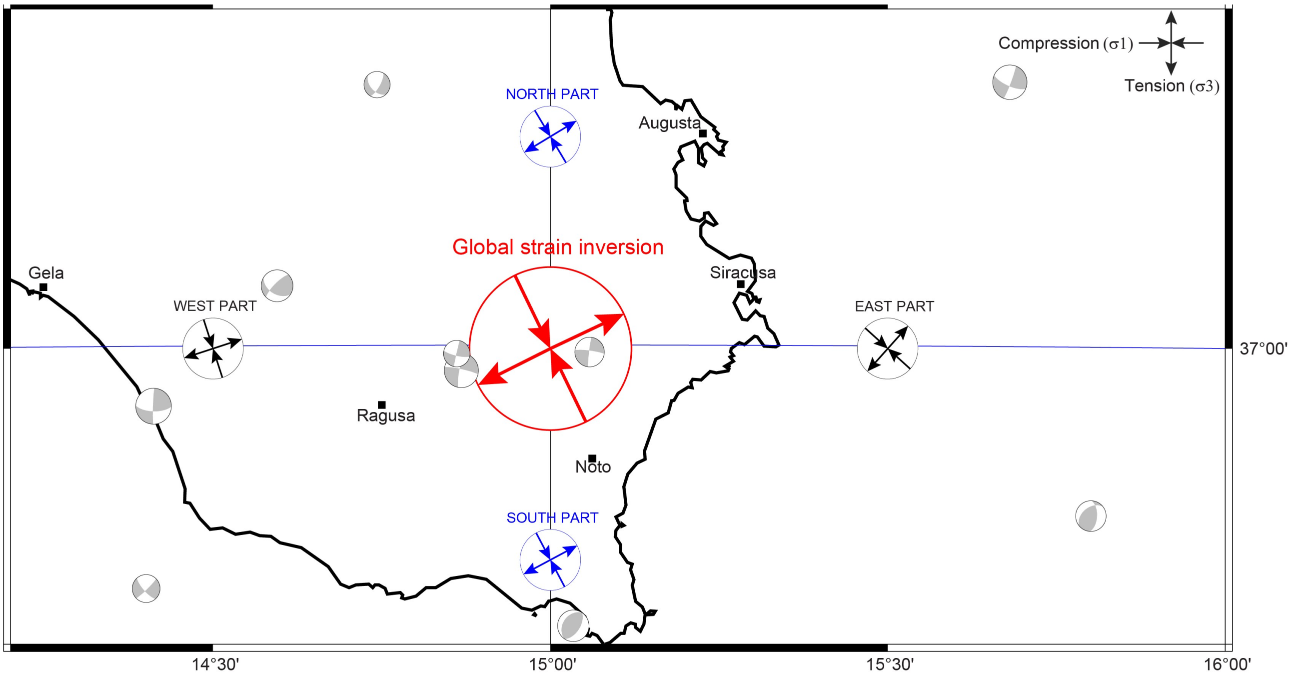

Supplementary Figure S7: *Focal mechanisms inversion over Southeastern Sicily using Mickael's method (Vavryčuk, 2014; Levandowski et al., 2018). The global strain inversion (red arrows) is consistent with local strain inversion performed on four subregions dividing SE Sicily. North and South subregions are delimited by the blue line. West and East subregions are delimited by the black line.*

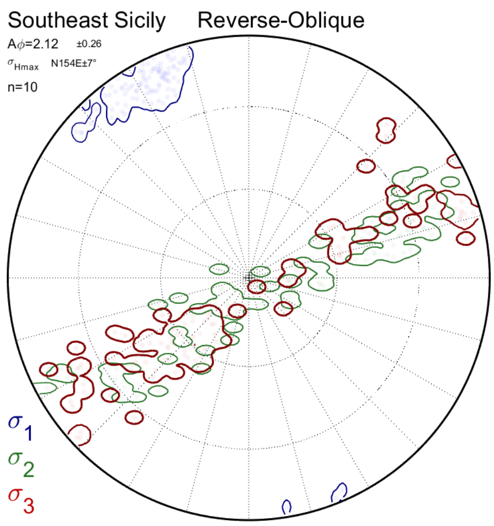

Supplementary Figure S8: *Global stress tensor of focal mechanisms of southeast Sicily (Figure 3 and Supplementary Figure S7) using the Mickael's method (Vavryčuk, 2014; Levandowski et al., 2018).*

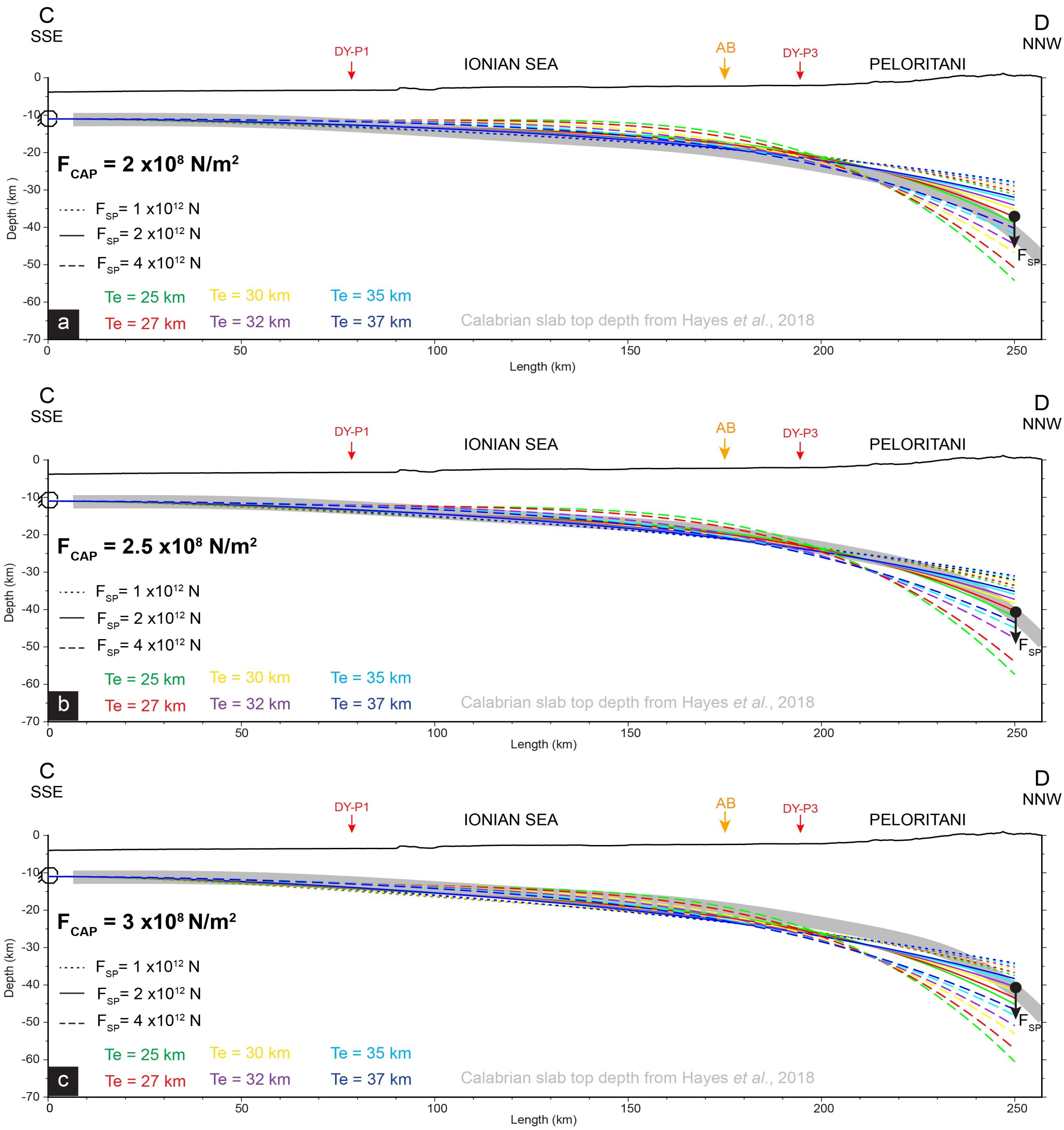

d Te \ F_{SP} / F_{CAP}	1×10^{12} N			2×10^{12} N			4×10^{12} N			
	2×10^8 N/m²	2.5×10^8 N/m²	3×10^8 N/m²	2×10^8 N/m²	2.5×10^8 N/m²	3×10^8 N/m²	2×10^8 N/m²	2.5×10^8 N/m²	3×10^8 N/m²	
25 km	2.4	1.5	2.2	1.4	0.8	2.3	4.2	4.5	5.4	RMS (km)
27 km	2.5	1.6	2.3	1.4	0.7	2.2	3.5	3.9	4.9	
30 km	2.6	1.8	2.3	1.4	0.7	2.2	2.6	3.1	4.2	
32 km	2.7	1.9	2.3	1.6	0.8	2.2	2.1	2.6	3.9	
35 km	2.9	2.0	2.4	1.8	1.0	2.2	1.5	2.1	3.5	
37 km	2.9	2.1	2.4	1.9	1.2	2.2	1.2	1.9	3.4	

Supplementary Figure S9: *Numerical models (gFlex from Wickert, 2016) of the oceanic lithosphere flexure were run with a broken plate with no-bending moment and no shear at the northern end of the CD profile, and a no-displacement condition at its southern end. The ante-Messinian cover and the CAP load are represented as a linear gradient with a maximum CAP load a) of 2×10^8 N/m², b) of 2.5×10^8 N/m², and c) of 3×10^8 N/m². We performed a slab pull of 1×10^{12} N (dashed lines), 2×10^{12} N (continuous lines), and 4×10^{12} N (dot-*

ted lines) bending of the oceanic lithosphere. We investigated elastic thickness (Te) of 25-37 km for the same model parameters. We represented the model with elastic thicknesses of 25 km (in green), 27 km (in red), 30 km (in yellow), 32 km (in purple), 35 km (in cyan), and 37 km (in blue) d) Misfit (RMS in km) of Calabrian slab top depth (Hayes, 2018) (in gray) interpolated on each model. The shaded cells are models represented in Figure 5.*

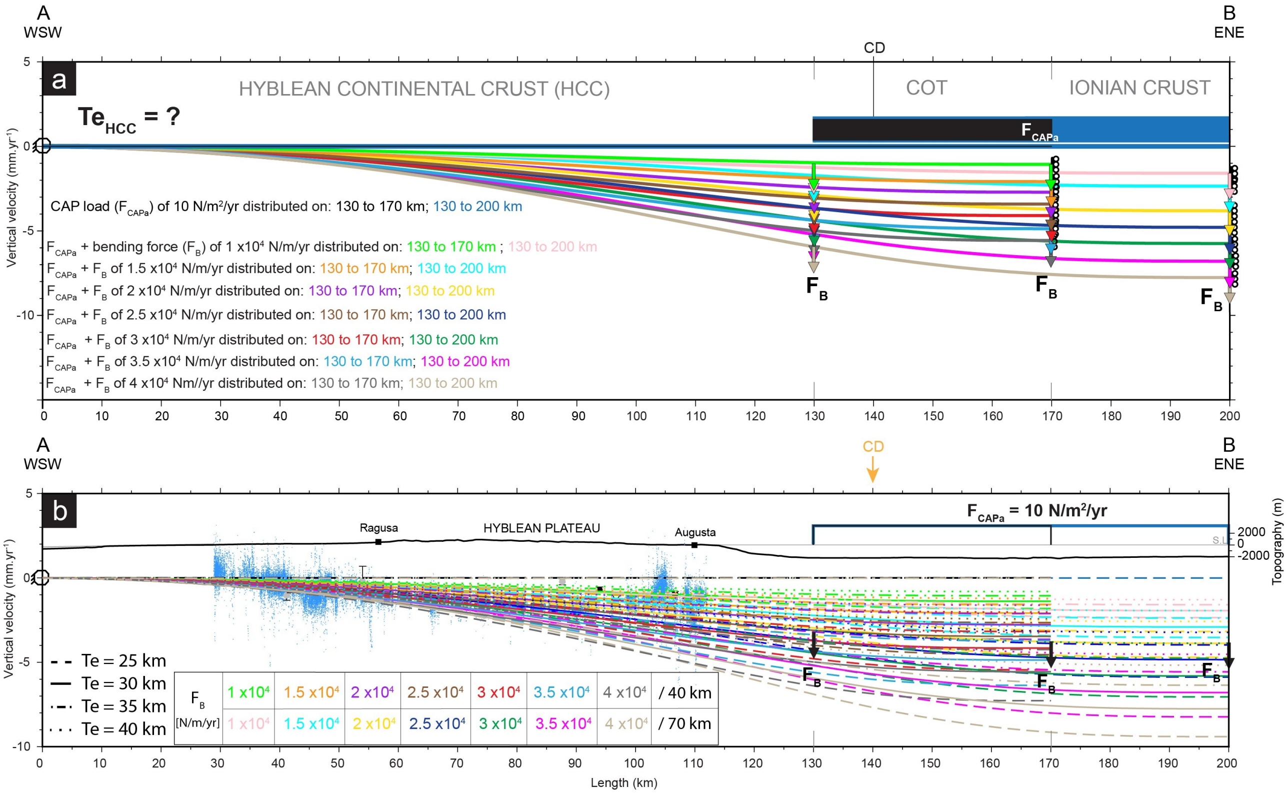

C — $F_{CAPa} + F_B$

Te	1 x10⁴ N/m/yr RMS InSAR (mm/yr)	1 x10⁴ N/m/yr RMS GNSS (mm/yr)	1.5 x10⁴ N/m/yr RMS InSAR (mm/yr)	1.5 x10⁴ N/m/yr RMS GNSS (mm/yr)	2 x10⁴ N/m/yr RMS InSAR (mm/yr)	2 x10⁴ N/m/yr RMS GNSS (mm/yr)	2.5 x10⁴ N/m/yr RMS InSAR (mm/yr)	2.5 x10⁴ N/m/yr RMS GNSS (mm/yr)	3 x10⁴ N/m/yr RMS InSAR (mm/yr)	3 x10⁴ N/m/yr RMS GNSS (mm/yr)	3.5 x10⁴ N/m/yr RMS InSAR (mm/yr)	3.5 x10⁴ N/m/yr RMS GNSS (mm/yr)	4 x10⁴ N/m/yr RMS InSAR (mm/yr)	4 x10⁴ N/m/yr RMS GNSS (mm/yr)	
25 km	0.7	0.8	0.5	1.1	0.5	1.4	0.9	1.7	1	2.1	1.3	2.4	1.6	2.7	130-170 km
30 km	0.8	0.7	0.6	0.9	0.4	1.2	0.5	1.4	0.7	1.7	0.9	2	1.2	2.3	
35 km	0.8	0.6	0.7	0.8	0.5	1	0.4	1.2	0.5	1.4	0.6	1.6	0.8	1.8	
40 km	0.9	0.5	0.8	0.7	0.6	0.8	0.5	0.9	0.4	1.1	0.4	1.3	0.5	1.4	
25 km	0.7	0.8	0.5	1	0.5	1.4	0.7	1.7	1	2	1.3	2.3	1.7	2.6	130-200 km
30 km	0.7	0.7	0.5	1	0.5	1.3	0.6	1.6	0.8	1.9	1.1	2.2	1.4	2.5	
35 km	0.8	0.7	0.6	0.9	0.5	1.1	0.5	1.4	0.7	1.7	0.9	1.9	1.1	2.2	
40 km	0.8	0.6	0.7	0.8	0.5	1	0.4	1.2	0.5	1.4	0.6	1.6	0.8	1.9	

Supplementary Figure S10: *a) Continental crustal flexure controlled by the retreat of the Ionian slab along the AB profile. We performed the only Calabrian accretionnary prism (CAP) load (F_{CAPa}) of 10 N/m²/yr (black line), the CAP load and the bending force (F_B) of 1 x10⁴ N/m/yr (light green line), 1.5 x10⁴ N/m/yr (orange line), 2 x10⁴ N/m/yr (purple line), 2.5 x10⁴ N/m/yr (brown line), 3 x10⁴ N/m/yr (red line), 3.5 x10⁴ N/m/yr (light blue line) or 4 x10⁴ N/m/yr (gray line) are distributed entirely on 1-km-long segments on the continent-ocean transition (COT), so 130 to 170 km of the AB profile. We test, then, the only CAP load (10 N/m²/yr) (blue line), the CAP load and the bending force of 1 x10⁴ N/m/yr (pink line), 1.5 x10⁴ N/m/yr (cyan line), 2 x10⁴ N/m/yr (yellow line), 2.5 x10⁴ N/m/yr (dark blue line), 3 x10⁴ N/m/yr (green line), 3.5 x10⁴ N/m/yr (magenta line) or 4 x10⁴ N/m/yr (light brown line) distributed on 1-km-long segments on the COT and western of the Ionian crust, so 130 to 200 km of the AB profile b) Numerical models (gFlex from Wickert, 2016) were run with no-displacement boundary condition at the southwestern profile end and a free displacement of a horizontally clamped boundary condition at the northeastern profile end. The CAP load and the bending force are performed from 130 to 200 km length (blue, pink, cyan, yellow dark blue, green, light blue and gray lines) and from 130 to 170 km length (black, light green, orange, purple, brown, red, magenta and light brown lines). Hyblean crustal flexure are performed with different elastic thickness of 25 km (dashed lines), 30 km (continuous lines), 35 km (dotted-dashed lines), and 40 km (dotted lines). Profile of PS-InSAR velocities Up (in blue) and GNSS velocities Up (NGL) with their uncertainties stacked in 20 km (in black) and 40 km (in gray) along the profile AB (see location in Figure 2). Topographic and bathymetric profile are presented without* *vertical exaggeration (VE=1). c) Misfit (RMS in mm/yr) of the PS-InSAR and GNSS (see b) interpolated on different models. The shaded cells are best models according to the RMS PS-InSAR value, and these models are represented in Figure 6b.*

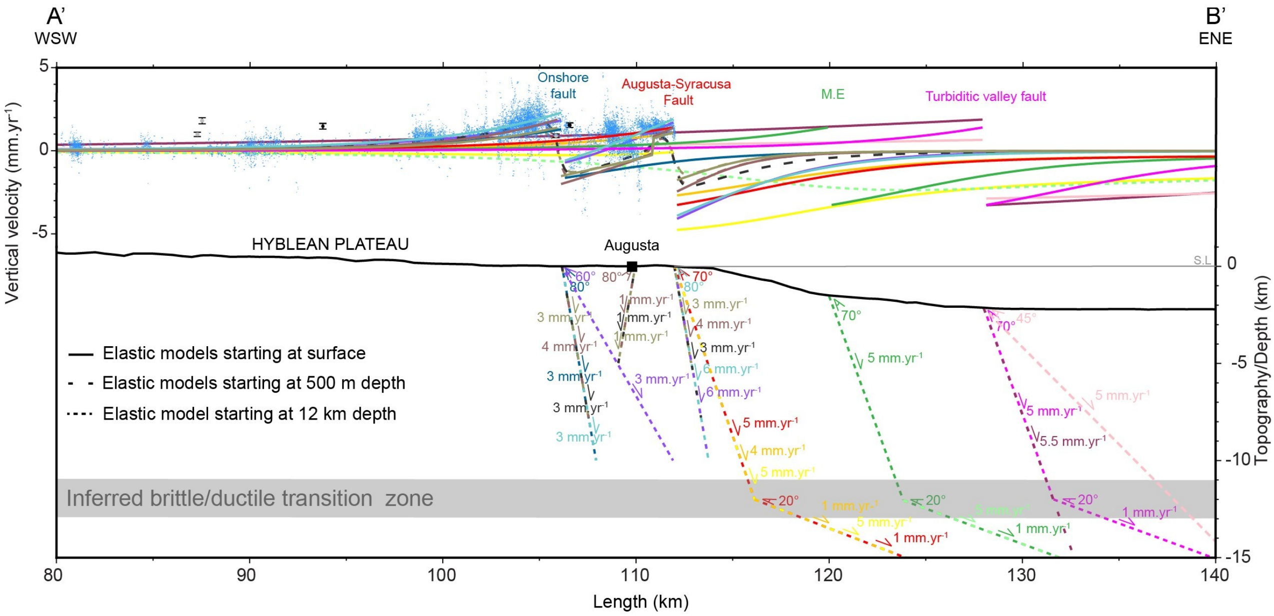

Supplementary Figure S11: *Interseismic loading numerical models (Coulomb 3.4) of offshore inferred active or active normals faults at the eastern Hyblean Platform have a step of 100 m. Profile of PS-InSAR velocities Up (in blue) are the reference frame for models, and were stacked across a 5 km width on both sides of the AB profile in Figure 7b (in blue). Modeled elastic deformation: the turbiditic valley normal fault identified by Gutscher et al., 2016 (magenta, dark pink and pink lines); the Malta Escarpment (M.E) (green and light green lines); the Augusta-Siracusa coastal fault (red, orange and yellow lines); onshore inferred active faults in Augusta (dark blue line). Modeled interseismic deformation: the Augusta-Siracusa coastal fault plus onshore inferred active faults are represented in light blue, dark and light brown lines). Topography/depth is represented without vertical exaggeration (V.E.x1).*

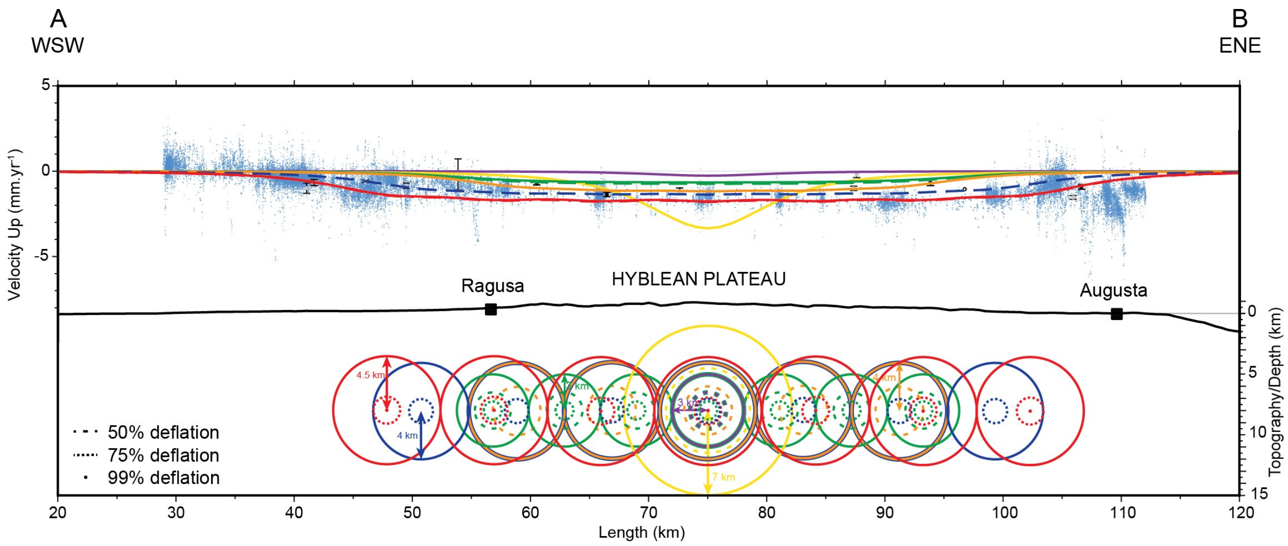

Supplementary Figure S12: *Volcanic material deflation model (Mogi, 1958) in central Hyblean Plateau. Volcanic material is represented by a sphere or several spheres located at 8 km depth according to Henriquet et al., 2019. A sphere of 3 km radius (in purple) and 7 km radius (in yellow) are tested with a 50% deflation (dashed line). Seven spheres of a 3 km radius (in green) have been constrained by 50% deflation (dashed line), and 75% deflation (dotted line). Five spheres of 4 km radius (in orange) were performed with 50% deflation (dashed line). Seven spheres of 4 km radius (in blue) were performed with 75% deflation (dotted line). Seven spheres of 4.5 km radius (in red) were performed with 75% (dotted line) and 99% (a point) deflation.*

Profile of PS-InSAR velocities Up (in blue) and GNSS velocities Up (NGL) with their uncertainties stacked in 20 km (in black) and 40 km (in gray) along the profile AB (see location in Figure 3). Topography/depth is represented without vertical exaggeration (V.E.x1).